Structural and Magnetic phase transitions in simple oxides using hybrid functionals

M. Alfredsson*, J.P. Brodholt, P.B. Wilson and G.D. Price

Department of Earth Sciences, University College London, Gower Street, London WC1E 6BT, UK

m.alfredsson@ucl.ac.uk

F. Corà

Davy Faraday Research Laboratory, The Royal Institution of GB, 21 Albemarle street, London W1C 4SE, UK

M. Calleja and R. Bruin

Department of Earth Sciences, Cambridge Univerisity, Downing street, Cambridge CB2 3EQ, UK

L. J. Blanshard and R.P. Tyer

Daresbury Laboratory, Daresbury, Warrington WA4 4AD, Cheshire, UK

Abstract

We present the structural as well as elastic properties of the alkaline earth oxides and FeO, calculated using hybrid exchange functionals within DFT. We show that by empirically fitting the amount of Fock-exchange in the hybrid functionals, we can accurately reproduce the pressure-induced phase transitions for MgO, CaO, SrO and BaO. For FeO the hybrid functionals predict an insulator_metal transition at ca. 150 GPa, associated with an i-B8_B8 structural phase transition. The structural phase transition is accompanied by a spin transition from a high- to low-spin electron configuration on the Fe^{2+} ions. Hence, FeO undergoes a magnetic phase transition from an anti-ferromagnetic to non-magnetic structure. We also find that as the ionicity of the polymorphs increases a higher fraction of Fock-exchange is required to reproduce the structural volumes reported from experiments.

Keywords: alkaline earth oxide, FeO, DFT, GGA, LDA, hybrid functional, CRYSTAL, phase transition, pressure

**)* corresponding author

1. Introduction

Despite its popularity among mineral physicists density functional theory (DFT) suffers from well-known shortcomings [1]:

1) The local density approximation (LDA) often underestimates experimentally reported volumes, while the generalised gradient approximation (GGA) functionals (e.g. PW91 and BLYP) overestimate the volumes (see for example *refs. 1-3*).
2) Because the values of calculated bulk moduli depend on the inverse equilibrium volumes, the LDA overestimates and the GGA techniques underestimate the experimentally reported values of bulk moduli [2,3].
3) LDA often underestimates, while GGA overestimates experimentally observed pressures of phase transitions [1,3,4].
4) DFT often fails in reproducing systems containing highly localised *d*- and *f*-electrons [1], including Fe containing minerals, such as Fe-silicates and oxides, wrongly predicting these minerals being metals, while they are in fact insulators.

Our approach to improve on the DFT accuracy is to use so called hybrid DFT exchange functionals. These are obtained by empirically mixing the DFT exchange with different amounts of Hartree-Fock exchange. The mixing coefficient can be treated as an empirical parameter, and chosen in such a way that calculated properties best reproduce available experimental observations. The best known hybrid DFT functional is Becke's 3-parameter exchange often used in combination with the Lee-Yang-Parr (LYP) correlation functional (B3LYP) [5,6]. In a previous study we have reported the success of hybrid functionals in modelling the B1 structure of FeO (wüstite) [7]. The hybrid functionals have also been successful in reproducing structural, electronic and magnetic properties of similar compounds, for example NiO [8-10], VO [11] and $BaTiO_3$ [12], and the performance of hybrid functionals in the solid state was recently reviewed by Corà et al. [13], including work on the related structures MnO and NiO studied by Middlemiss and Mackrodt. We here extend our work on structural and elastic properties, to include the performance of hybrid functionals in describing structural and magnetic phase transitions. Only one study has, to our knowledge, been published using hybrid functionals to study phase

transitions [14]. Here we present results for five different oxides, namely: FeO, BaO, SrO, CaO and MgO.

All five oxides discussed here are stable in the B1 or a rhombohedrally distorted B1 (r-B1) structure at zero temperature and pressure. However, as we increase the pressure they undergo different phase transitions as schematically shown in ***Fig. 1***. In particular, MgO (periclase), CaO (lime) and SrO show a B1_B2 phase transition [15-22] (***Fig. 1a***) that has been frequently studied in the literature employing different computational techniques (see for example *refs. 3 and 18-22*). MgO may exist in the lower mantle of the Earth, and, is thus, expected to be one of the most common minerals in the Earth [23]. CaO is an important material used for construction work and in steel manufacturing [24,25]. Lime is also utilised for arsenic removal; as softener in drinking water; and for flue gas treatment [25]. Here, we have chosen to study CaO because it has a well-characterised B1_B2 phase transition, reported to occur at around 60 GPa [15,16 19-22, 26]. Experimental studies on MgO have only been possible up to ca. 200 GPa, in which range no phase transition is reported [27]. From theoretical studies the phase transition in MgO is predicted to occur at pressures between 450 and 660 GPa [3,18,21,28-30]. For comparison we will also discuss the B1 to B2 transition in SrO, which is experimentally [17] and theoretically [3,19-22] reported to occur at around 36 GPa.

BaO has at least two experimentally observed structural phase transitions B1_*i*-B8_PH_4I (***Fig. 1b***) at 10 and 15 GPa, respectively, and eventually a third transition between the PH_4I_B2 structures at pressures above 60 GPa [31,32]. In the B1 structure, both cations and anions are in octrahedrally coordinated sites. In the *i*-B8 structure the anions remain octrahedrally coordinated, while the cations are in a bi-pyramidal site still with six nearest neighbour anions. In the PH_4I structure the cations are instead coordinated to eight anions, of which four are slightly closer to the cations than the other four. As the pressure increases, however, the anion-cation distances approach those of the B2 structure, in which the cation is in a symmetric 8-fold coordinated sites. The increase of coordination number as the pressure increases, suggests that the oxide becomes more ionic at higher pressures.

At zero temperature and pressure FeO is stable in the r-B1 structure, but transforms into a B8 or *i*-B8 structure at higher pressures [33,34]. It has also been suggested that the *i*-B8 and B8 polymorphs may co-exist [34,35]. Above the Néel temperature (198 K at ambient pressure [36]) FeO also has the B1 structure, and is iso-structural with the alkaline earth oxides. Experimentally the B1 structure is proposed to transform into a B8 polytype at ca. 96 GPa and 700 K [33], while the r-B1 to B8-type of transition has not yet been experimentally characterised.

One common feature of systems containing transition metal ions is the possibility to change from high-spin (HS) to low-spin (LS) states. For FeO it is, therefore, not only important to investigate the structural variations as a function of pressure, but also possible spin transitions that give rise to different magnetic structures. In this paper we discuss the anti-ferromagnetic (AFM) and non-magnetic (NM) structures of FeO (see ***Fig. 1c***). In the anti-ferromagnetic B1 and r-B1 structures, the Fe^{2+} ions have a high-spin configuration with four un-paired electrons (Fe^{2+} is a d^6 ion), which give rise to a magnetic moment on the Fe^{2+} ions. In these structures the magnetic moments are aligned within the [111] plane [37], as indicated in ***Fig 1c***. It has also been proposed that the high-pressure polymorphs, *i*-B8 and B8, show AFM structures [35,38], in which the magnetic moments are aligned within the [110]-planes (see ***Fig. 1c***). In a Mössbauer study by Pasternak et al. [39] it was proposed that the high-spin configuration of the Fe^{2+} ions undergoes a spin transition to a low-spin configuration at ca. 120 GPa. A low spin state results in a non-magnetic structure, since the Fe^{2+} ions in this situation have no un-paired electrons. On the other hand, in an XES study by Badro et al. [40] this HS to LS transition was not observed at pressures up to 140 GPa. Hence, one suitable application of the hybrid functionals is to investigate whether an HS to LS transition can occur in FeO as a function of pressure, and to understand if this transition is associated with metallisation.

2. Methods

All calculations were performed with the CRYSTAL 2003 code (CR03) [41]. In this program the crystalline orbitals are expressed as linear combinations of Bloch functions, which in turn are built up from Gaussian-type orbitals (GTO). In CR03, periodic Self-Consistent-Field (SCF) calculations can be performed both within the

Hartree-Fock (HF) scheme, as well as with various functional formulations within density functional theory (DFT). Not only is it possible to combine different exchange and correlation functionals, it is also possible to mix the HF and DFT exchange functionals to any desired degree. We can, therefore, use different exchange ratios to investigate different observables, such as the electronic and geometric structures of the oxides. The latter approach provides us a computationally tractable way to study strongly correlated systems, including FeO [7,13].

In this paper we mix the Hartree-Fock (F; also referred to as the Fock-exchange) with the Slater (S) [42], Becke(B) [5] or Perdew-Wang 91 (P) [43] exchange functionals, in combination with the Vosko-Wilk-Nusair (VWN) [44], Lee-Yang-Parr (LYP) [6] or Perdew-Wang91 (PW91) [43] correlation functionals. The generic hybrid functional with a percentage α of Fock-exchange is indicated with the shorthand notation $F_{\alpha}X_{100-\alpha}C$, where X and C are the acronyms of the DFT exchange and correlation functionals employed, as indicated above. For example, $F_{35}B_{65}LYP$ will represent:

$$F_{35}B_{65}LYP = 35X(F) + 65X(B) + C(LYP), \quad (1)$$

α can be treated as an empirical parameter, allowing us to monitor how the calculated properties vary by tuning the α-value between 0 and 100%. This procedure allows us to select the α-value that best reproduces the experimental observables. All calculations for FeO are spin polarised.

The exchange-correlation potential was expanded numerically, and the cut-off threshold parameters (ITOLs) for the selection of the Coulomb and Exchange integrals were set to {8 8 8 8 16}. We used a k-point mesh of 10x10x10, expanded according to the Monkhorst-Pack scheme. The Broyden mixing, as implemented in CR03 [41], was employed for the metallic solutions, while for the insulating solutions we employed the level shifting technique [45] for faster convergence. In all calculations we used the same all-electron basis set for oxygen, *i.e.* 8-411Gd1 [46]. For the cations we used all-electron basis sets for Mg (8-611Gd1 [46]), Ca (86-511Gd3 [3]) and Fe (86-411d41 [47]), while for Sr and Ba we used Hay-Wadt's small

core effective core potentials (ECP) in combination with the 31Gd3 [3] and 31Gd1 [3] gaussian-type of valence basis sets for Ba and O, respectively. The GTOs employed in our study are optimised in the B1 structure, and we did not re-optimise the basis sets for the different polymorphs, as was instead done in *ref. 3*. We should, however, bear in mind that basis set effects may be important when determining phase transition pressures.

All structure optimisations are performed at constant pressure, employing the DOMIN-algorithm [48], which is a BFGS-method, to optimise the lattice parameters. To optimise the atomic positions we instead use the Berny-algorithm [49]. Both the DOMIN- and Berny-algorithms are implemented in the CR03 code.
For calculations at constant pressure we have optimised the enthalpy (H):

$$H = E + PV, \tag{2}$$

of the system, where E is the internal energy, V the volume and P the pressure (not to be mistaken with the symbol P indicating the PW91 exchange functional).

The pressures associated with the various phase transitions were obtained using two different techniques. For CaO, BaO and FeO we fitted the calculated enthalpy values for each polymorph to a 5^{th}-order polynomial of pressure. At the phase transition the enthalpy difference ($\Delta H_T(P)$) fullfills the condition:

$$\Delta H_T(P)=H_A(P)-H_B(P)=0 \tag{3}$$

where $H_A(P)$ and $H_B(P)$ denote the calculated enthalpies for the two polymorphs (A and B) at the given pressure.

For comparison with *ref. 3* we also calculated the transition pressure (P_T) between the B1_B2 polymorphs of MgO, CaO and SrO starting from the Murnaghan equation of state [50], which yields the internal energy according to:

$$E_{Murn}(V) = -E_0 + \frac{B_0 V}{B'}\left[\frac{(V_0/V)^{B'}}{B'-1} + 1\right] - \frac{V_0 B_0}{B'-1}, \quad (4)$$

where E_0 and V_0 denote the equilibrium energy and volume, and B_0 and B' are the bulk modulus and its derivative, respectively. With the knowledge that

$$P = -\frac{\partial E}{\partial V} \quad (5)$$

we can express the enthalpy as function of pressure according to:

$$H(P) = E_0 + \frac{V_0 B}{B'-1}\left[\left(\frac{B'}{B}P + 1\right)^{1-\frac{1}{B'}} - 1\right] \quad (6)$$

The calculated bulk moduli are obtained by fitting the Murnaghan equation of state.

Scanning the phase diagram of one mineral is in general computationally very expensive, since it includes a range of calculations at different pressures for all the possible magnetic and structural polymorphs. For some compounds we are required to perform between 50-100 calculations per functional to determine the phase diagram solely as a function of pressure. In this project we have particularly taken advantage of the Condor-cluster, which is built and maintained at UCL. In this cluster we have access to more than 900 MS-Windows based machine, and because our calculations are independent on each other, we can submit all jobs we need to determine the phase diagram of one compound at the same time. After analyses our data are stored at the SRB vaults available within the E-minerals project. Currently these vaults are located at the Daresbury Laboratory, Cambridge University and UCL in London. This solution also makes it easy for other groups to access the stored data, and it facilitates collaborations between the different groups within the project.

3. Results on MgO, CaO and SrO

3.1 Effect of Exchange and Correlation functional on V_0 and B_0

In this section we describe how the mixing of different amounts of Fock-exchange (α) in combination with the different exchange (B, P and S) and correlation (LYP, PW91 and VWN) DFT functionals influences the optimised bulk volumes and moduli. We discuss CaO in detail because it is the compound for which we have the most accurate experimental and theoretical data available.

Our first aim is to determine how the different *correlation functionals* (VWN, LYP and PW91) reproduce the experimentally reported volumes and bulk moduli in combination with the $F_\alpha B_{100-\alpha}$ hybrid exchange functionals. The optimised geometries (V_0) and bulk moduli (B_0) at zero pressure for CaO, obtained from Murnaghan's equation of state (equation 4), are reported in ***Fig. 2***. For comparison we also calculated V_0 and B_0, without any correlation functional.

Independently on the correlation functional chosen, we see from ***Fig. 2a*** that all the equilibrium volumes become smaller as the amount of Fock-exchange (α) increases, but for the same value of α the PW91-correlation functional gives the smallest and the VWN-functional the largest volume. We also find that all three correlation functionals reduce V_0 compared to a functional with no correlation. These observations are the same for both the B1 and B2 structures; however, in ***Fig. 2a*** we see that, for each functional, the errors compared to the experimental values in the equilibrium volumes for the B1 and B2 structures are different. Furthermore, we find that the B2 structure in general requires more Fock-exchange than the B1 structure to correctly reproduce the experimentally reported V_0 values of 24.6 and 27.8 Å [15], respectively.

As shown in ***Fig. 2b***, increasing the amount of Fock-exchange increases the value of the bulk moduli. As expected the larger values of V_0 give rise to a smaller B_0 in both the B1 and B2 structures, and consequently, the Becke exchange-functional without any correlation gives rise to smaller bulk moduli than the functionals containing electron correlation.

Let us now examine the effect of different formulations of the DFT *exchange functional* in the hybrid. In order to do this, we fix the correlation functional to its PW91 formulation, and vary the type of exchange functional in the hybrid. Results are

plotted in ***Fig. 3***. When comparing the two GGA functionals (B and P), we find very little difference in the V_0 and B_0 values for the B1 structure. Both curves show smaller V_0 and higher B_0 values as α increases.

However, using the LDA functionals (Slater exchange and VWN-correlation) in the hybrid functional ($F_\alpha S_{100-\alpha}$VWN) produces smaller volumes compared to the $F_\alpha B_{100-\alpha}$VWN functionals (see ***Fig. 3a***). Interestingly, the volumes increase as the amount of Fock-exchange increases, which is the opposite behaviour to that observed with the GGA exchange functionals. As a consequence B_0 becomes smaller as α increases (see ***Fig. 3b***) for the $F_\alpha S_{100-\alpha}$VWN functionals, but larger for the $F_\alpha B_{100-\alpha}$VWN functionals.

The B2 structures, in which cation and anion have higher coordination number, are expected to be more ionic than the B1 structure; as we have seen, the B2 structure needs a higher percentage of Fock-exchange to correctly reproduce the experimental V_0 values (see ***Fig. 2a***). The explanation for the need of more Fock-exchange is due to the competition between the long-ranged electrostatic and the short-ranged covalent contributions; when increasing the amount of Fock-exchange we obtain a more localised solution which give rise to a higher Madelung-field, which is in better agreement with the true solution for the ionic compounds than the more delocalised (and thus covalent) solution obtained using pure DFT.

Since also the cation type modifies the ionicity of the solid, we include in our investigation how the cation type influences the V_0 and B_0 values. This can be achieved by comparing MgO, CaO and SrO. We expect the ionicity to decrease according to MgO>CaO>SrO because we find that the 3-d orbitals show important hybridisation with the neighbouring oxygens already for Ca. In this study we only include the $F_\alpha B_{100-\alpha}$LYP hybrid functionals. As demonstrated in ***Fig. 4a*** again the V_0 values decrease as the percentage of Fock-exchange increases. The same behaviour is observed for all three oxides, but the amount of Fock-exchange required for reproducing the experimental volumes decreases as the size of the cation increases: MgO needs ca. 40% and SrO 0% Fock-exchange to reproduce the experimental values of 18.5 Å [51] and 34.3 Å [17], *i.e.* again we find that the more ionic the structure, the more Fock-exchange is required to reproduce the experimental data. B_0

values are again following the trends in V_0 and are getting smaller as α increases (see ***Fig. 4b***).

3.1.2 B1_B2 Phase Transitions in MgO, CaO and SrO

At this point we turn to investigate how the transition pressure (P_T) for the pressure-induced B1_B2 phase transition in the alkaline earth oxides is predicted by using the hybrid functionals. In ***Fig. 5*** we present the value of P_T calculated employing three different $F_\alpha B_{100-\alpha}$ combinations in the $F_\alpha B_{100-\alpha}$LYP series, and the SVWN (LDA) functionals. As discussed in the introduction, the GGA-methods, including BLYP, often overestimate P_T in comparison to experiment. It is, therefore, not surprising to find that this is also the case in our calculations on CaO, where BLYP predicts a P_T value of ca. 84 GPa, compared with an experimental value of ca. 60 GPa [15,26]. Increasing the amount of Fock-exchange in the hybrid slightly reduces the calculated pressure of the phase transition, bringing it closer to the experimental value. Nevertheless, the best agreement with the experimental value is obtained using the LDA functional (SVWN), i.e. the one that yields the worst agreement for the equilibrium volumes.

We also calculated P_T from Murnaghan's equation of state (see equation 6); these results are presented in **Table 1**. Firstly, we note that the two methods employed in our investigation (compare **Table 1** and ***Figs. 5a-c***) give good agreement with each other when the same exchange and correlation functionals are combined. We also find that, as the amount of Fock-exchange increases, P_T decreases. Only for the combinations between Fock- and Slater exchange ($F_\alpha S_{100-\alpha}$VWN) is it found that P_T increases as the amount of Fock-exchange increases, thus, following the same behaviour as previously discussed for V_0.

In ***Fig. 6*** we show that P_T decreases in the order of MgO>CaO>SrO. Moreover, in ***Fig. 6*** we observe that as α increases for CaO and SrO, P_T decreases. In contrast, MgO exhibits a different behaviour with a maximum in P_T for α around 60%. All calculated P_T values (450-550 GPa) are in good agreement with previous theoretical

investigations, which found a range of values for P_T from 450 to 660 GPa [*e.g.* 3,18,21,28-30].

4. B1_ B8_ PH_4I_B2 Phase Transitions in BaO

Most theoretical investigations on the phase transitions in BaO have focused on the B1_B2 transition, while only two theoretical studies have investigated the full experimentally proposed sequence B1_*i*-B8_PH_4I_B2. One used plane-wave calculations [52], and the second a sophisticated inter-atomic potential model (AIM) [53]. Experimentally Weir et al. [31] and Liu et al. [32] proposed that the B1 structure at room temperature undergoes a phase transition to an *i*-B8 structure at ca. 10 GPa, and then transforms into a PH_4I type of structure at ca. 15 GPa. The latter structure can be regarded as a distorted B2 structure, and indeed as the pressure increases the extent of the distortion decreases and the PH_4I structure strives towards the B2.

In this study we employ different Hamiltonians, namely BLYP, $F_{35}B_{65}$LYP, $F_{50}B_{50}$LYP and LDA, to study the full sequence of phase transitions proposed experimentally. Optimising the enthalpies as a function of pressure we determine the phase transition by fitting the function ΔH_T to a 5^{th} order polynomial (equation 3). As for CaO, we here find that that as the amount of Fock-exchange increases the pressure of the predicted phase transitions decrease (see **Table 2**).

We start with the B1 to *i*-B8 phase transition, which is experimentally observed at ca. 10 GPa. Uludo_an et al. [52] performed plane-wave calculations with the PW91 functional, and reported the phase transition to occur at ca 11 GPa, while our P_T value using the BLYP functional is 20 GPa. Considering the P_T values for CaO reported in **Table 1**, we notice that the phase transition pressure calculated with the PW91 functional is lower than that predicted with the BLYP; comparison between the B1 to *i*-B8 transition pressure calculated here with the results of *ref. 52* is consistent with this trend. However, since GGA functionals usually overestimate the P_T-values we suggest that the excellent agreement between *ref. 52* and the experimental value by Weir et al. [31] could also be associated with the choice of pseudo-potentials used in *ref. 52*. Our $F_{50}B_{50}$LYP functional predicts this phase transitions to occur at ca. 18

GPa, while the LDA Hamiltonian predicts a P_T value of 5 GPa. In *ref. 53* the pressure of the phase transition was estimated as *ca.* 12 GPa using the AIM model.

For the *i*-B8_PH_4I transition the hybrid functionals yield similar P_T values as the BLYP functional (P_T~27 GPa), while the LDA Hamiltonians predicts a phase transition at ca. 13 GPa. The experimental value given in *ref.* [31] is about 15 GPa, while the calculated values in *refs. 52* and *53* are of 22 and 19 GPa, respectively. Again the P_T value obtained with the PW91 functional [52] is lower than the P_T value calculated at the BLYP level.

The last BaO phase suggested to exist in the experimental study is the high-symmetry B2. This has not been directly observed, but the distorted PH_4I gradually evolves towards the B2 structure on increasing pressure. The PH_4I_B2 phase transition can therefore take place in two ways: either via an abrupt (first-order) phase transition, or via a gradual (second-order) evolution of the PH_4I structure towards the higher symmetry B2 phase. A computational study can help us answering this question: in the former case the calculated enthalpy of the two phases will cross as a function of pressure; in the latter, the calculated enthalpy of the PH_4I phase will tend asymptotically to that of the B2 structure, without crossing it. Experimental evidence [31] shows that, in the range of pressure examined, the PH_4I structure constantly approaches the B2 structure, and the latter was not actually observed since the experiments only reached pressures of 60 GPa. Our calculations, with each of the four functionals employed, predict the existence of a first-order PH_4I_B2 phase transition. The transition pressure is calculated as ca. 62 GPa at the BLYP level, while the hybrid functionals anticipate the phase transition at 44 to 48 GPa. The calculated P_T value for the LDA functional is 50 GPa. In the paper by Uludo_an et al. [52] the PH_4I_B2 P_T was predicted at *ca.* 62 GPa. On the other hand, the AIM study by Aguado et al. [53] predicted the same transition to occur at only 25 GPa, employing lattice static calculations. The reasons the latter authors calculate a lower P_T is discussed in ref. 53, one explanation is that the AIM potential is not accurate enough to differentiate between the small energy differences associated with the different polymorphs. Nevertheless, all the computational studies agree in predicting the existence of a PH_4I_B2 transition. This observation, however, does not rule out the possibility of a gradual evolution of the PH_4I into the B2 phase. Again, calculations provide a suitable

tool to investigate this topic. The distortion leading from the PH_4I to B2 structure is characterised by two structural parameters: firstly the c/a ratio, which equals $1/\sqrt{2}$ (~0.705) in the B2 phase while is higher in the distorted PH_4I, and secondly the fractional coordinate of the cation, which is (_,0,_) in the B2 and (_,0,_+Δ) in the PH_4I structure. We have studied the evolution of both c/a ratio and of the parameter Δ as a function of pressure.

The c/a ratio is known also from the experimental work, and Weir et al. [31] showed that the c/a-ratio slowly approaches the $1/\sqrt{2}$-value (~0.705), which is characteristic for the B2 structure, on increasing pressure. In ***Fig. 7*** we demonstrate that the BLYP, as well as the hybrid functionals, predict a decreasing value of c/a as function of pressure, in agreement with experiment, but in none of the functionals the c/a ratio has yet reached the $1/\sqrt{2}$ value at 70 GPa, which is the highest pressure we considered. Our results are in excellent agreement with the AIM-values obtained by Aguado et al. [53], using molecular dynamics simulations (at room temperature) even though all theoretical values are underestimated compared to the experimental ones. This observation may be related to kinetic effects, which change the energy barriers for the atomic displacements. However, we want to emphasise that it can be either the MD simulations; the experimental work or both which are underestimating the entropy effects since both investigations are done at relatively low temperatures.

Investigating the lattice parameters (*a*- and *c*-axes) separately we find that the *c*-axis shows the largest compressibility, changing from 3.6 to 3.05 Å, corresponding to *ca.* 15%, while the *a*-axis shows a change of *ca.* 7.5% (see ***Fig. 8***). At zero pressure we find that both the *a*- and *c*-axes are overestimated compared to the experimental values, but as the pressure increases we find good agreement between calculated and experimental ones. At 14 GPa the lattice parameters are 4.375 and 3.25 Å [31] for the *a*- and *c*-axes, respectively.

Let us now examine the change that occurs in the parameter Δ, representing the displacement of the Ba ion in the PH_4I phase, as a function of pressure. The parameter Δ is zero in the B2 structure (see ***Fig. 9***). At 70 GPa we find that the Δ-values are between 0.07 and 0.08 for the different functionals, while at zero pressure they are

roughly 0.17 fractional units. Experimentally the Δ-value is 0.06 at 60 GPa [20]. As for the c/a-ratio (see ***Fig. 7***), using the $F_{50}B_{50}$LYP functional the parameter Δ approaches its value in the B2 phase more rapidly than with the BLYP and the $F_{35}B_{65}$LYP functionals, suggesting that the phase transition should be observed at lower P_T when the amount of Fock-exchange increases, which is in line with the behaviour observed for the other phase transitions.

5. *i-B8(AFM)_ B8(NM)* Phase Transition in FeO

In **Table 3** we report pressure transitions between the high-pressure structures of B8-type in FeO, considering the four different FeO polymorphs: *i*-B8(AFM); *i*-B8(NM); B8(AFM); and B8(NM). We have in this case employed six different functionals. The aims of the current study on FeO are to: *i*) determine a possible HS to LS transition on the Fe^{2+} ions; and *ii*) establish if the high-pressure structures are metallic.

From our calculations we find that the enthalpy differences between the *i*-B8(AFM) and B8(AFM), as well as the B8(NM) polymorphs are indeed small, but for each functional, the *i*-B8(AFM) polymorph is predicted to be energetically the most stable one at pressures higher than 90 GPa. This finding is in agreement with previous theoretical investigations [35,38]. Yet the enthalpy differences are small, and we can, therefore, not rule out the possibility of co-existing polymorphs discussed in *refs. 34* and *35*. Consequently, the phase transitions listed in **Table 3** could be expected to occur over a broad pressure range. We also show that the pressure-induced phase transition predicted using the different functionals is the same, namely an *i*-B8(AFM)_B8(NM) transition at P>90 GPa, which means that the structural phase change is associated with a magnetic phase transition, involving a HS to LS transition on the Fe^{2+} ions. Hence, our calculations predict a spin breakdown in the range of 145 to 190 GPa, depending on the functional. We would like to emphasise that the pressures associated with the *i*-B8(AFM) to B8(NM) transitions from our CR03 calculations are lower than the pressure reported by Cohen et al. [54] using a GGA functional. The latter authors reported a spin break down at ca. 200 GPa calculated in for B1 structure, using the Stoner model. One fundamental difference between our calculations and those reported in *ref. 54* are that we report a spin-break down

associated with a structural phase transitions, while in *ref. 54* the spin break down is associated with one and the same structure, the B1 structure, which in fact is the low-pressure structure.

As for the previous oxides discussed in this paper we find that the gradient-corrected functionals (BLYP and PW91) result in higher P_T than the LDA (SVWN) functional. This is also the case for FeO (see ***Fig. 11***), but while for CaO, SrO and BaO we found that as the amount of Fock-exchange increases P_T decreases, the case for FeO is different, as can bee seen from ***Figs. 11e*** and ***f***. $F_{50}B_{50}$LYP exhibits a higher P_T than $F_{35}B_{65}$LYP. FeO shows therefore a similar behaviour to MgO, with a maximum in P_T as α increases (see ***Fig. 6***). Bearing in mind that the low-spin configuration of the Fe^{2+} ion has a similar ionic size and properties as the Mg^{2+} ion, this behaviour is not entirely surprising, but we also believe that the similarity of MgO and FeO needs to be studied in more detail elsewhere.

The density-of-states (DOS) from all functionals investigated show that the *i*-B8(AFM) structure is insulating, while the B8(NM) is metallic (see ***Fig. 10***). Hence, the *i*-B8(AFM)_B8(NM) is also coupled with an insulator to metal transition. The origin of the metallisation is due to an important overlap between the Fe*3d* and O*2sp* crystal orbitals, which is associated with the higher symmetry of the B8(NM) than the *i*-B8(AFM) structure. Experimentally the high-pressure polymorph of FeO is reported as being metallic [55].

6. Summary and Conclusions

Below we summarise our findings, concerning the performance of hybrid functionals:

- By empirically fitting the amount of Fock-exchange in combination with different exchange and correlation functionals, we can reproduce the structural and elastic properties of all the oxides studied here. The issue was discussed in detail by Corà et al. [13], who concluded that the more ionic a compound the more Fock-exchange is required to reproduce the experimentally observed structural parameters, while to correctly reproduce the bulk moduli only between 20-30% Fock-exchange is required. Similar results were reported by Alfredsson et al. [7], and by Bredow et al. [10]. This is consistent with the fact

that the B2 structure requires more Fock-exchange than the B1 structure. It also explains why the smaller and more ionic cations (Mg^{2+} and Ca^{2+}) require more Fock-exchange than the larger but less ionic Sr^{2+} cation.

- The hybrid functionals reproduce values of the transition pressures in between the P_T values obtained using the GGA and LDA Hamiltonians, following the trends observed for the equilibrium volumes. However, the P_T values are more difficult to reproduce than V_0 and B_0, since they depend on small energy and enthalpy differences.
- In contrast to structural and elastic properties, for which we found that the hybrid functionals containing Slater-exchange are in poor agreement with experiment, the $F_\alpha S_{100-\alpha}$VWN hybrid functional is an attractive alternative to determine the transition pressure of oxides including heavy cations, such as SrO.
- We have also shown that the hybrid functionals correctly reproduce both insulators as well as metals, which imply that hybrid functionals can be successfully used to study insulator_metal transitions, such as the *i*-B8(AFM)_B8(NM) transition in FeO. This structural phase transition is associated with a magnetic phase transition. Hybrid functionals are able to reproduce the subtle changes in the structure associated with spin transitions.
- Using the Condor-cluster available at UCL in London, the real time required to study phase transitions is reduced from years to months. All data are effectively stored in the SRB vaults available in the E-minerals project.

Acknowledgement

The authors would like to thank W.C. Mackrodt and D. Middlemiss for valuable discussions. We acknowledge financial support from NERC (NER/T/S/2001/00855; Environment from the molecular level) and computer resources at University College London (UCL). F.C. acknowledge an Advanced EPRCS fellowship.

References:

[1] R.M. Martin, *'Electronic structure – basic theory and practical methods'*, Cambridge University press, Cambridge, UK (2004), *and ref. there in*

[2] A. Zupan and M. Causa, *Int. J. Quantum Chem.*, **56**, 337 (1995)

[3] M.-P. Habas, R. Dovesi and A. Lichanot, *J. Phys.: Condens. Matter,* **10**, 6897 (1998)

[4] N. Moll, M. Bockstedt, M. Fuchs, E. Pehlke and M. Scheffler, ***Phys. Rev. B***, **52**, 2550 (1995)

[5] A.D. Becke, *J. Chem. Phys.*, 98, 5648 (1988)

[6] C. Lee, W. Yang and R.G. Parr, *Phys. Rev. B*, **37**, 785 (1988)

[7] M. Alfredsson, G.D. Price, C.R.A. Catlow, R. Orlando, S.C. Parker and J.P. Brodholt, *Phys. Rev. B* (2004) *in press*

[8] F. Illias and R.L. Martin, *J. Chem. Phys.*, **108**, 2519 (1998)

[9] I. de P. R. Moreira, F. Illas and R.L. Martin, *Phys. Rev. B*, **65**, 155102 (2002)

[10] T. Bredow and A.R. Gerson, *Phys. Rev. B*, **61**, 5194 (2000)

[11] W.C. Mackrodt, D.S. Middlemiss and T.G. Owens, *Phys. Rev. B*, **69**, 115119 (2004)

[12] F. Corà *Mol. Phys.* (2004), *in press*

[13] F. Corà, M. Alfredsson, G. Mallia, D. S. Middlemiss, W. C. Mackrodt, R. Dovesi and R. Orlando, 'The performance of hybrid density functionals in solid state chemisty', J. McGrady and N. Kaltsoyannis ed., Density Functional Theory in Inorganic Chemistry, Structure and Bonding, Vol. XX, Springer-Verlag, Heidelberg, *in press*

[14] N. Wilson and J. Muscat, *Mol. Sim.*, **28**, 903 (2002)

[15] P. Richet, H.K. Mao and P.M Bell, *J. Geophys. Res. (Solid Earth)*, **93**, 15 279 (1986)

[16] Y. Sato and R. Jeanloz, *J. Geophys. Res.*, **86**, 1773 (1981)

[17] J.F. Mammone, H.K. Mao and P.M. Bell, *Geophys. Res. Lett.*, **8**, 140 (1981)

[18] A.R. Oganov, M.J. Gillan and G.D. Price, *J. Chem. Phys.*, **118**, 10174 (2003)

[19] M.J. Mehl, R.E. Cohen and H. Krakauer, *J. Geophys. Res. (Solid Earth)*, **93**, 8009 (1988)

[20] M.J. Mehl, R. Hemley and L.L. Boyer, *Phys. Rev. B*, **33**, 8685 (1986)

[21] P. Cortona and A.V. Monteleone, *J. Phys.: Condens. Matter*, **8**, 8983 (1996)

[22] C.E. Sims, G.D. Barrera, N.L. Allan and W.C. Mackrodt, *Phys.Rev. B*, **57**, 11164 (1998)

[23] S.I. Karato, '*The dynamic structure of the deep Earth*', Princeton University Press, Princeton, US (2003)

[24] F.A. Cotton and G. Wilkinson, *Advanced Inorganic Chemistry; A comprehensive text*, 4th ed., John-Wiley & Sons: New York (1980)

[25] The National Lime Association; *www.lime.org*

[26] R. Jeanloz, T.J. Ahrens, H.K. Mao and P.M Bell, *Science*, **206**, 829 (1979)

[27] T.S. Duffy, R.J. Hemley and H.K. Mao, *Phys. Rev. Lett.*, **74**, 1371 (1995)

[28] A.R.Oganov and P.I. Dorogokupets, *Phys. Rev. B*, **67**, 224110 (2003)

[29] N.D. Drummond and G.J. Ackland, *Phys. Rev. B*, **65**, 184104 (2002)

[30] B.B. Karki, L. Stixrude, S.J. Clark, M.C. Warren, G.J. Ackland and J. Crain, *Am. Mineral.*, **82**, 51 (1997)

[31] S.T. Weir, Y.K. Vohra and A.L. Ruoff, *Phys. Rev. B*, **33**, 4221 (1986)

[32] L. Liu and W.A. Bassett, *J. Geophys. Res.*, **77**, 4934 (1972)

[33] Y. Fei and H.K. Mao, *Scicence*, **266**, 1678 (1994)

[34] M. Murakami, K. Hirose, S. Ono, F. Tsuchiya, M. Isshiki and T. Watanuki, *Phys. Earth and Plant. Inter.*, (2004) *article in press*

[35] I.I. Mazin, Y. Fei, R. Downs and R. Cohen, *Am. Miner.*, **83**, 451 (1998)

[36] H. Bizette, *Ann. Phys.*, **1**, 295 (1946)

[37] N.C. Tombs and H.P. Rooksby, *Nature*, **165**, 442 (1950)

[38] Z. Fang, I.V. Solovyev, H. Sawada and K. Terakura, *Phys. Rev. B*, **59**, 762 (1999)

[39] M.P. Pasternak, R.D. Taylor, R. Jeanloz, X. Li, J.H. Nguyen and C.A. McCammon, *Phys. Rev. Lett.*, **79**, 5046 (1997)

[40] J. Badro, V.V. Struzhkin, J. Shu, R.J. Hemley and H.K. Mao, *Phys. Rev. Lett.*, **83**, 4101 (1999)

[41] V.R. Saunders, R. Dovesi, C. Roetti, R. Orlando, C.M. Zicovich-Wilson, N. M. Harrison, K. Doll, B. Civalleri, I. J. Bush, Ph. D'Arco and M. Llunell, CRYSTAL03, User's Manual, University of Turin, Turin, Italy (2003)

[42] P. A. M. Dirac, *Proc. Cambridge Phil. Soc.*, **26**, 376 (1930)

[43] J. P. Perdew, Y. Wang, *Phys. Rev. B*, **33**, 8800 (1986); J.P. Perdew and Y. Wang, *Phys. Rev. B*, **40**, 3399 (1989); J. P. Perdew and Y. Wang, *Phys. Rev. B*, **45** 13244

(1992); J. P. Perdew 'Electronic structure of Solids 1991', Akademie Verlag, Berlin (1991)
[44] S.H. Vosko, L. Wilk and M. Nusair, *Can. J. Phys.*, **58**, 1200 (1980)
[45] M.F. Guest and V.R. Saunders, *Mol. Phys.*, **28**, 819 (1974)
[46] M.I. McCarthy and N.M. Harrison, *Phys. Rev. B*, **49**, 8574 (1994)
[47] Towler 1992, www.chimifm.unito.it/teorica/crystal/Basis_Sets/iron.html
[48] P. Spellucci, *Math. Prog.*, **82**, 413 (1998); www.mathematik.tu-darmstadt.de/ags/ag8/Mitglieder/spellucci_de.html
[49] H.B. Schlegel, *J. Comp. Chem.*, **3**, 214 (1982)
[50] F.D. Murnaghan, *Proc. Natl. Acad. Sci. USA*, **30**, 244 (1944)
[51] R.W.G. Wyckoff, Crystal Structures, 2nd ed. Vol. 1, Interscience; (John Wiley & Sons, Inc), New York, (1965)
[52] M. Uludo_an, T. Ca_in, A. Strachan and W.A. Goddard III, *J. Compt.-Aided Mat. Design*, **8**, 193 (2001)
[53] A. Aguado, L. Bernasconi and P.A. Madden, *J. Chem. Phys.*, **118**, 5704 (2003)
[54] R.E. Cohen and I.I. Mazin and D.G. Isaak, *Science*, **275**, 654 (1997)
[55] E. Knittle and R. Jeanloz, *Geophys. Res. Lett.*, **13**, 1541 (1986)
[56] O.L. Anderson and P. Jr Andreatch, *J. Am. Ceram. Soc.*, **49**, 404 (1966)

Table 1 Transition pressures (P_T) for B1_B2 transition in CaO, using different functionals. P_T is calculated from equation 6. Pressures are given in GPa, and α denotes the amount of Fock-exchange in percentage.

α	$F_\alpha B_{100-\alpha}$LYP	$F_\alpha B_{100-\alpha}$PW91	$F_\alpha B_{100-\alpha}$VWN	$F_\alpha P_{100-\alpha}$PW91	$F_\alpha S_{100-\alpha}$VWN
0	84	73	87	73	65
20	82	71	88	71	69
40	80	70	86	70	74
60	78	68	84	68	75
80	76	67	81	67	76
100	72	65	78	65	78
Expt.[15]	60				

Table 2 Pressure transitions (P_T) for the B1_*i*-B8_PH_4I_B2 phase transitions in BaO calculated for different Hamiltonians using eq. 3. Comparisons are made to the experiment and other theoretical studies.

Hamiltonian	P_T (GPa) B1→*i*-B8	P_T (GPa) *i*-B8→PH_4I	P_T (GPa) PH_4I→B2
BLYP	20	26	62
$F_{35}B_{65}$LYP	19	27	49
$F_{50}B_{50}$LYP	18	27	44
LDA	5	13	50
PW91[52]	11	22	62
AIM[53]	12	19	25
Expt.[31]	10	15	>60

Table 3 Pressure transitions (P_T) in FeO calculated for different Hamiltonians using eq. 3.

Hamiltonian	P_T (GPa) B8(AFM)→ *i*-B8(AFM)	P_T (GPa) *i*-B8(AFM)→ B8(NM)
BLYP		181
$F_{35}B_{65}$LYP	68	145
$F_{50}B_{50}$LYP	85	155
B3LYP	25	192
PW91[52]		213
LDA		150

Figure Captions

Fig. 1 Proposed structural phase transitions for ***a)*** MgO, CaO and SrO; ***b)*** BaO; and ***c)*** FeO. Arrows indicate increasing pressure. Light grey and dark grey balls indicate oxygen ions and cations, respectively. For FeO planes with opposite spins are marked with dotted and full lines. The B8 structure discussed in the text is derived from the i-B8 structure, by changing the atomic positions for the oxygen ions and cations.

Fig. 2 Optimised ***a)*** volumes and ***b)*** bulk moduli (at zero pressure) as a function of Fock-exchange (α) for CaO, using different correlation functionals combined with $F_{\alpha}B_{100-\alpha}$ exchange functional. Closed and open shapes represent the B1 and B2 structures, respectively. Experimental values from *refs.15, 16 and 26*.

Fig. 3 Optimised ***a)*** volumes and ***b)*** bulk moduli for B1 structure of CaO, using different combinations of exchange and correlation functionals. Experimental values from *refs. 16* and *26*

Fig. 4 Optimised ***a)*** volumes and ***b)*** bulk moduli for the B1 structures of MgO, CaO and SrO, using the $F_{\alpha}B_{100-\alpha}$LYP functionals. Experimental values are taken from *refs. 16,17,51 and 56.*

Fig. 5 Transition pressures (P_T) for CaO using the ***a)*** BLYP; ***b)*** $F_{35}B_{65}$LYP; ***c)*** $F_{50}B_{50}$LYP; and ***d)*** SVWN functionals. P_T calculated from eq. 3.

Fig. 6 Transition pressures (P_T) for the B1_B2 transition in MgO, CaO and SrO. The experimental value of CaO and SrO are 60 GPa [15,26] and 36 GPa [17], respectively. All calculations are performed with the $F_{\alpha}H_{1-\alpha}$LYP functionals.

Fig. 7 c/a ratio for the PH_4I structure of BaO as a function of pressure.

Fig. 8 Optimised *a*- and *c*-axes as function of pressure for the PH_4I structure of BaO. Closed and open shapes represent *a*- and *c*-axes, respectively. Experimental values from *ref. 31*.

Fig. 9 Δ-value as function of pressure for the PH_4I structure of BaO. Experimental value from *ref. 31*.

Fig. 10 Total density-of-states (DOS) for the ***a)*** *i*-B8(AFM); and ***b)*** B8(NM) structures at 140 GPa, using the $H_{35}B_{65}$LYP functional.

Fig 1

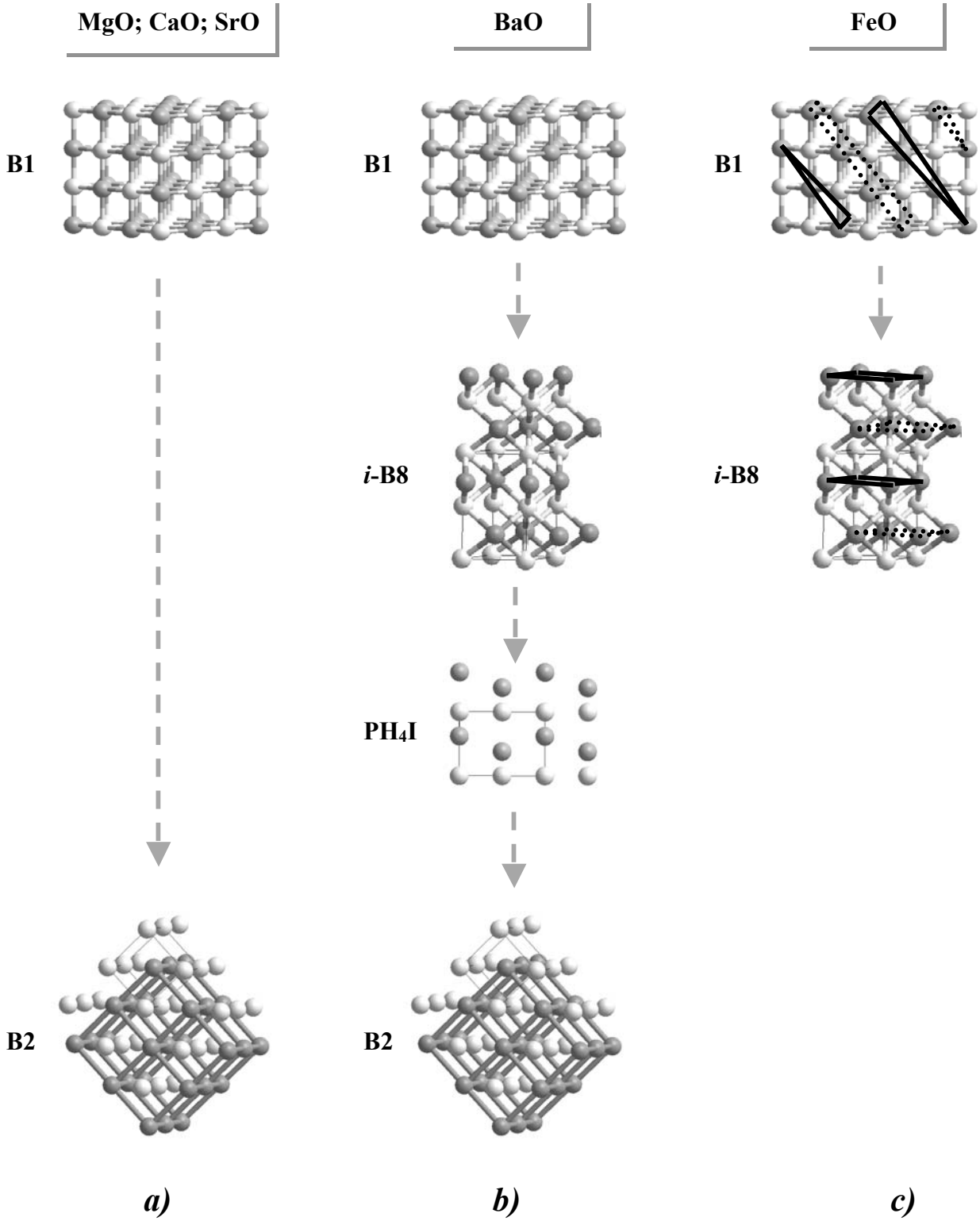

Fig. 2a

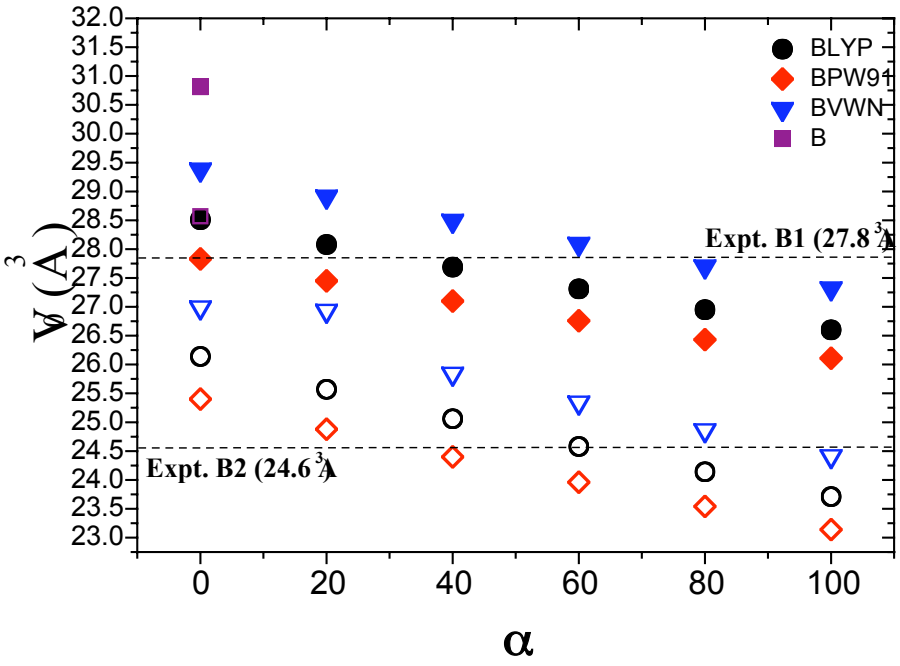
V (Å^3)
α
Expt. B1 (27.8 Å^3)
Expt. B2 (24.6 Å^3)
BLYP
BPW91
BVWN
B

Fig. 2b

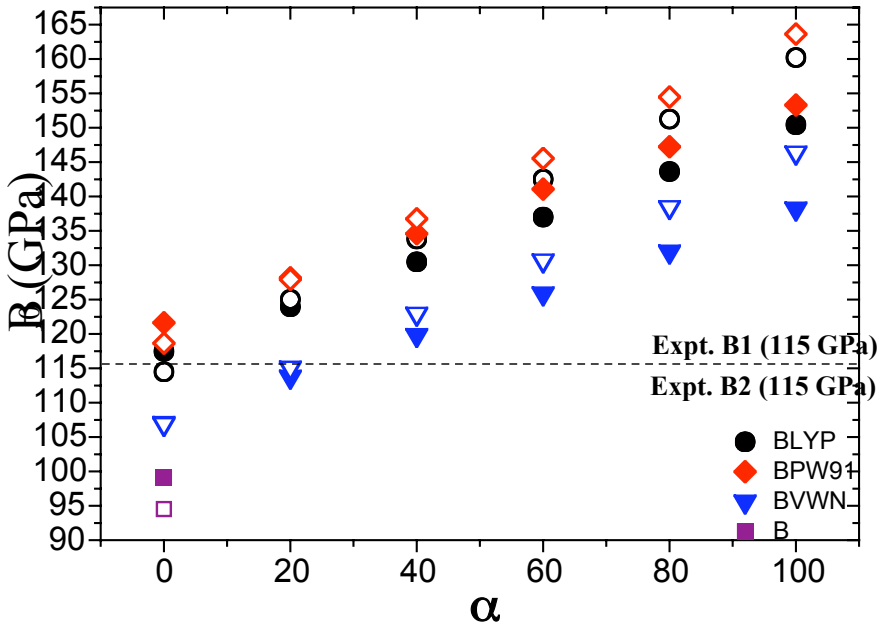
B (GPa)
α
Expt. B1 (115 GPa)
Expt. B2 (115 GPa)
BLYP
BPW91
BVWN
B

Fig. 3a

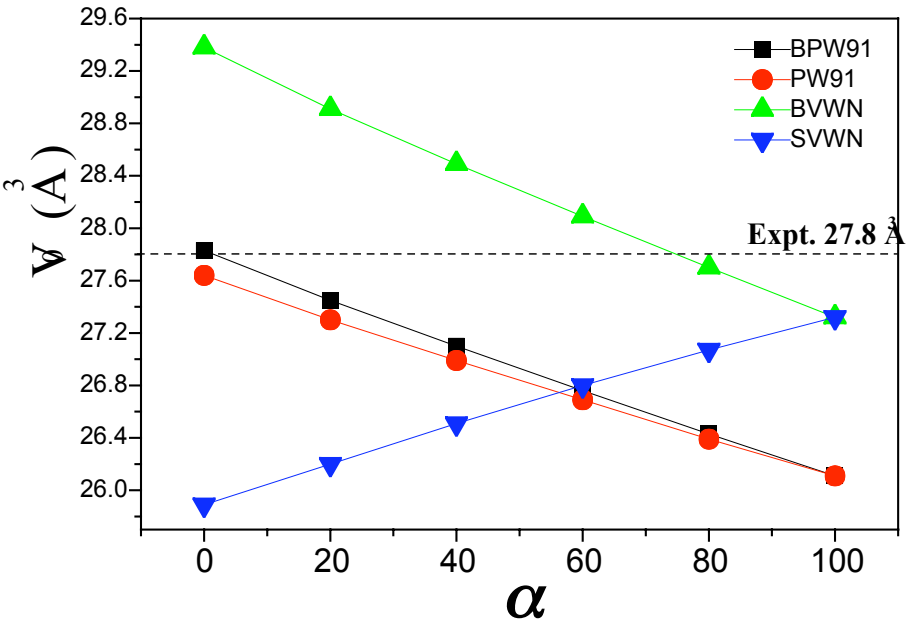
BPW91
PW91
BVWN
SVWN
Expt. 27.8 Å
V (Å)
α

Fig. 3b

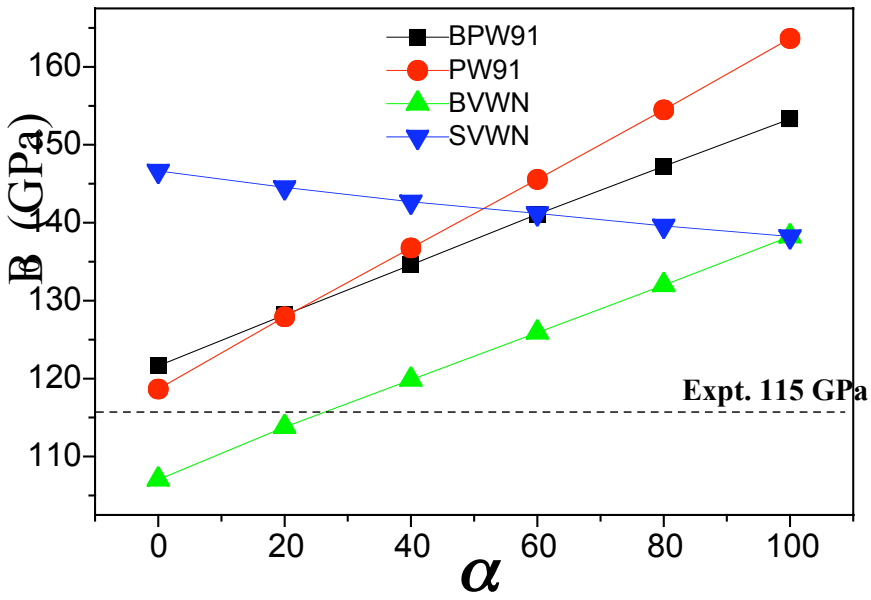
BPW91
PW91
BVWN
SVWN
Expt. 115 GPa
B (GPa)
α

Fig. 4a

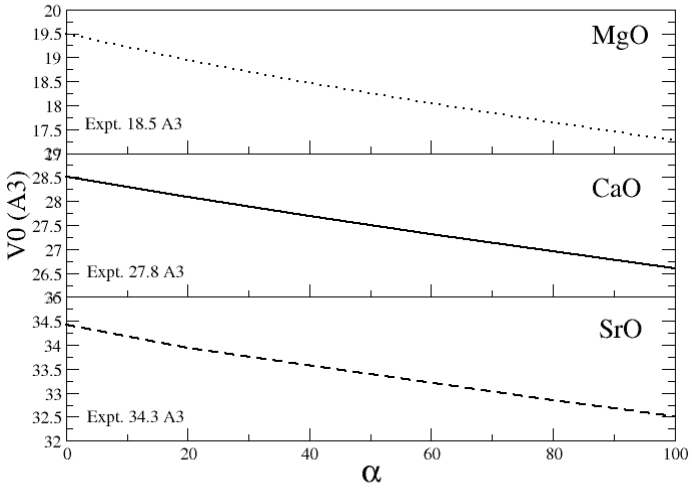
MgO
Expt. 18.5 A3
CaO
Expt. 27.8 A3
SrO
Expt. 34.3 A3
V0 (A3)
α

Fig. 4b

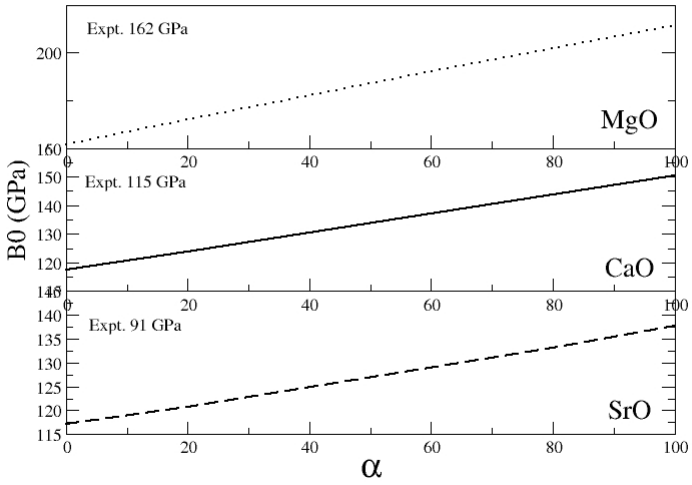
Expt. 162 GPa
MgO
Expt. 115 GPa
CaO
Expt. 91 GPa
SrO
B0 (GPa)
α

Fig. 5

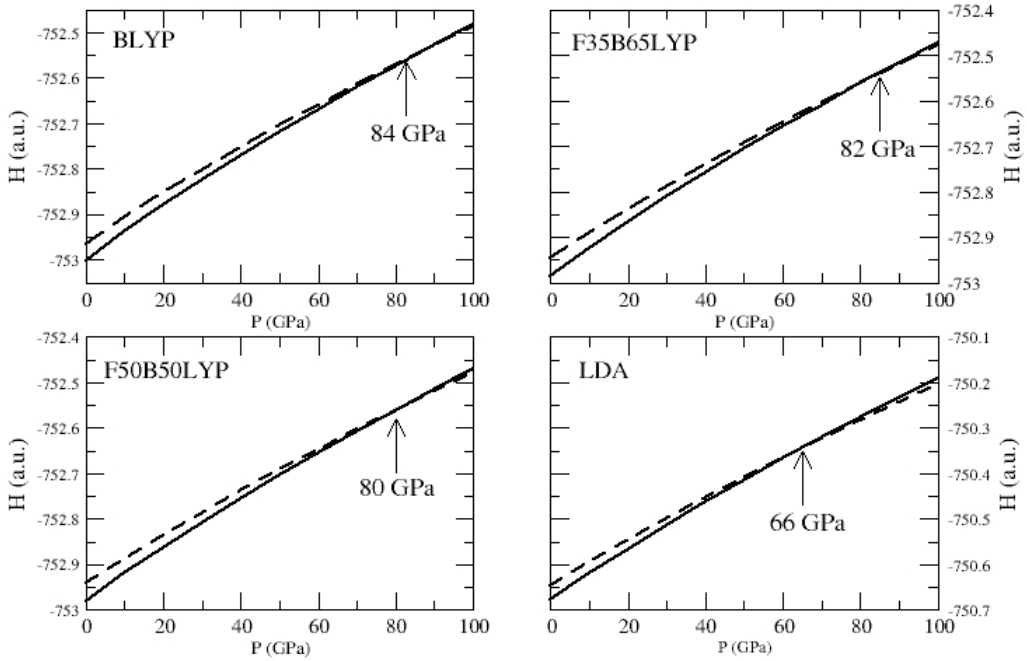
BLYP
84 GPa
F35B65LYP
82 GPa
F50B50LYP
80 GPa
LDA
66 GPa
H (a.u.)
P (GPa)

Fig. 6

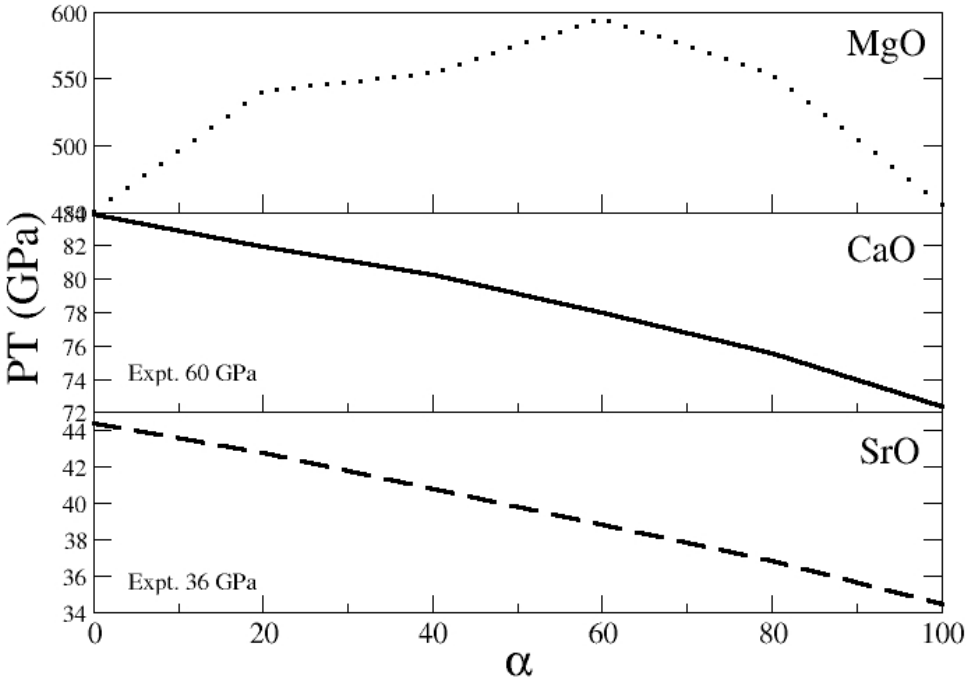
MgO
CaO
SrO
Expt. 60 GPa
Expt. 36 GPa
PT (GPa)
α
600
550
500
82
80
78
76
74
72
44
42
40
38
36
34
0
20
40
60
80
100

Fig. 7

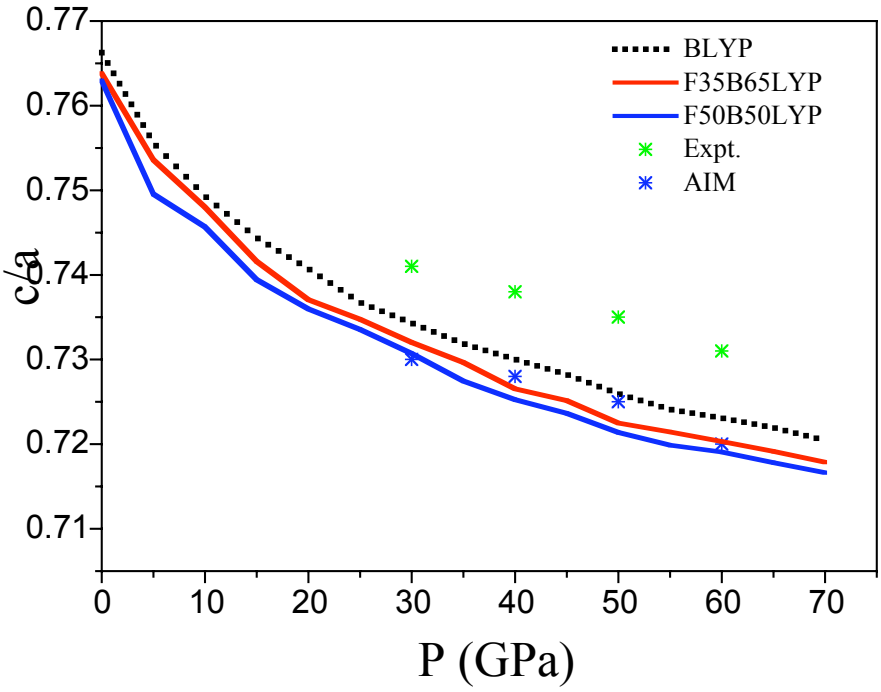
0.77
0.76
0.75
0.74
0.73
0.72
0.71
c/a
0
10
20
30
40
50
60
70
P (GPa)
BLYP
F35B65LYP
F50B50LYP
Expt.
AIM

Fig. 8

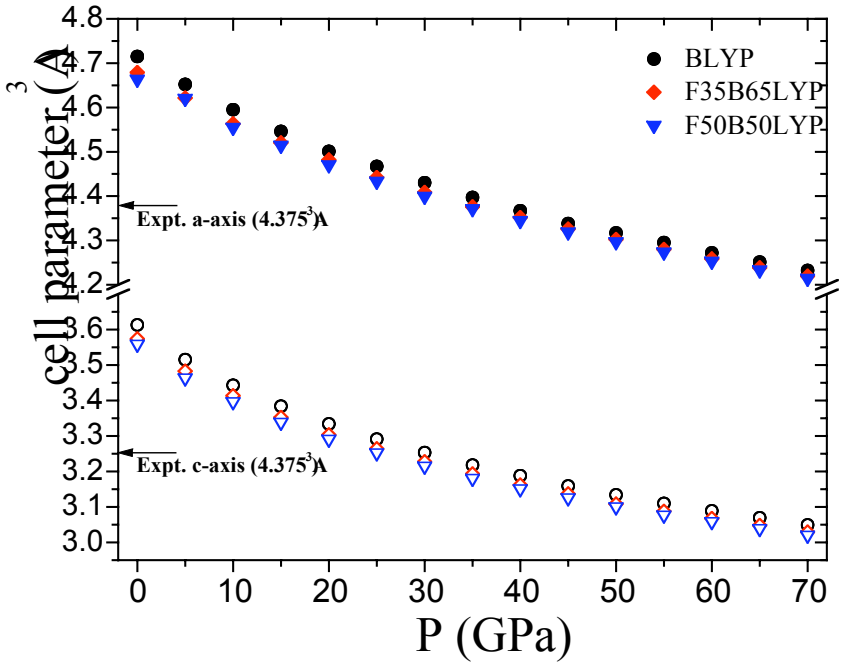
BLYP
F35B65LYP
F50B50LYP
Expt. a-axis (4.375 Å)
Expt. c-axis (4.375 Å)
cell parameter (Å)
P (GPa)
4.8
4.7
4.6
4.5
4.4
4.3
4.2
3.6
3.5
3.4
3.3
3.2
3.1
3.0
0
10
20
30
40
50
60
70

Fig. 9

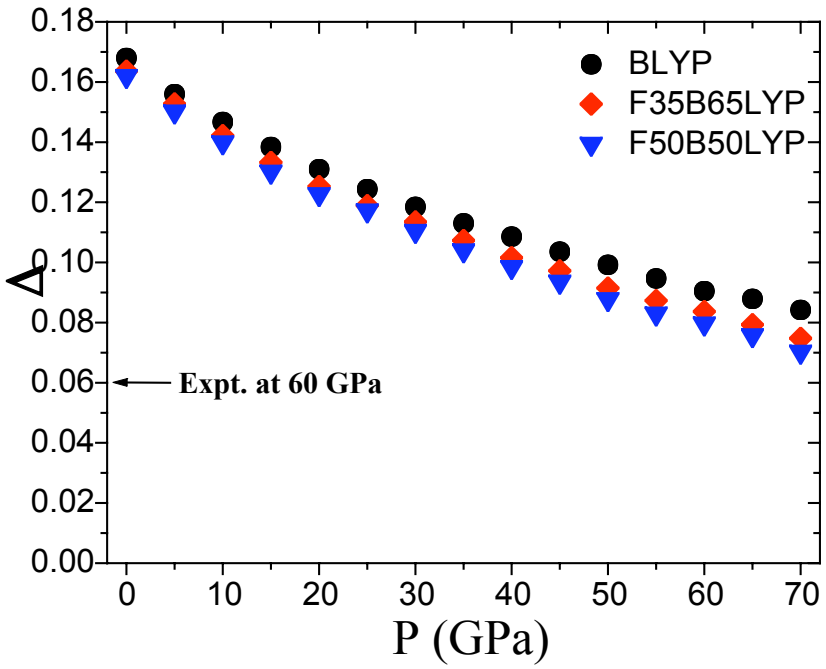
0.18
0.16
0.14
0.12
0.10
0.08
0.06
0.04
0.02
0.00
Δ
BLYP
F35B65LYP
F50B50LYP
Expt. at 60 GPa
0
10
20
30
40
50
60
70
P (GPa)